Supporting Information

Stability of Zeolites in Aqueous Phase Reactions

Sebastian Prodinger[a], Hui Shi[a], Sebastian Eckstein[b], Jian Zhi Hu[a], Mariefel V. Olarte[a], Donald M. Camaioni[a], Miroslaw A. Derewinski[a]* and Johannes A. Lercher[a,b]*

[a] Institute for Integrated Catalysis, Pacific Northwest National Laboratory, P.O. Box 999, Richland, WA 99352 (United States)

[b] Department of Chemistry and Catalysis Research Institute, TU München, Lichtenbergstrasse 4, 85748 Garching (Germany)

Table of Content

X-ray diffraction

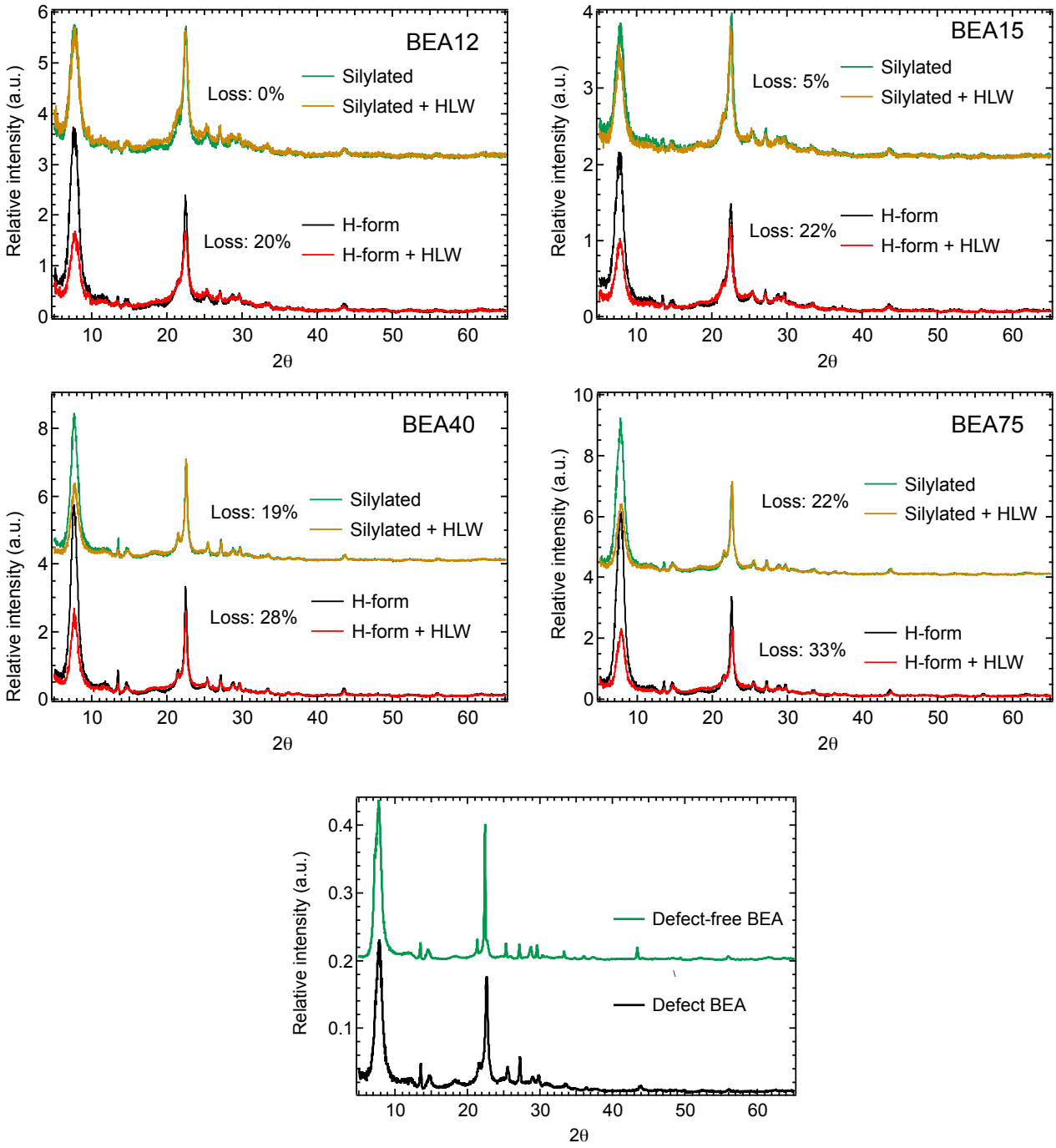

Figure S1. X-ray diffractograms of parent and silylated BEA before and after the interaction with hot liquid water for extended periods of time. Notice, that the integrity of the framework, as measured by the loss in peak area denoted in the legend, suffers extensively in the parent materials compared to the silylated version. Diffraction peak areas were calculated using simple peak fitting. The diffractograms for the defect-BEA and defect-free BEA are also presented, both show reflections attributed to the BEA framework.

N_2 physisorption

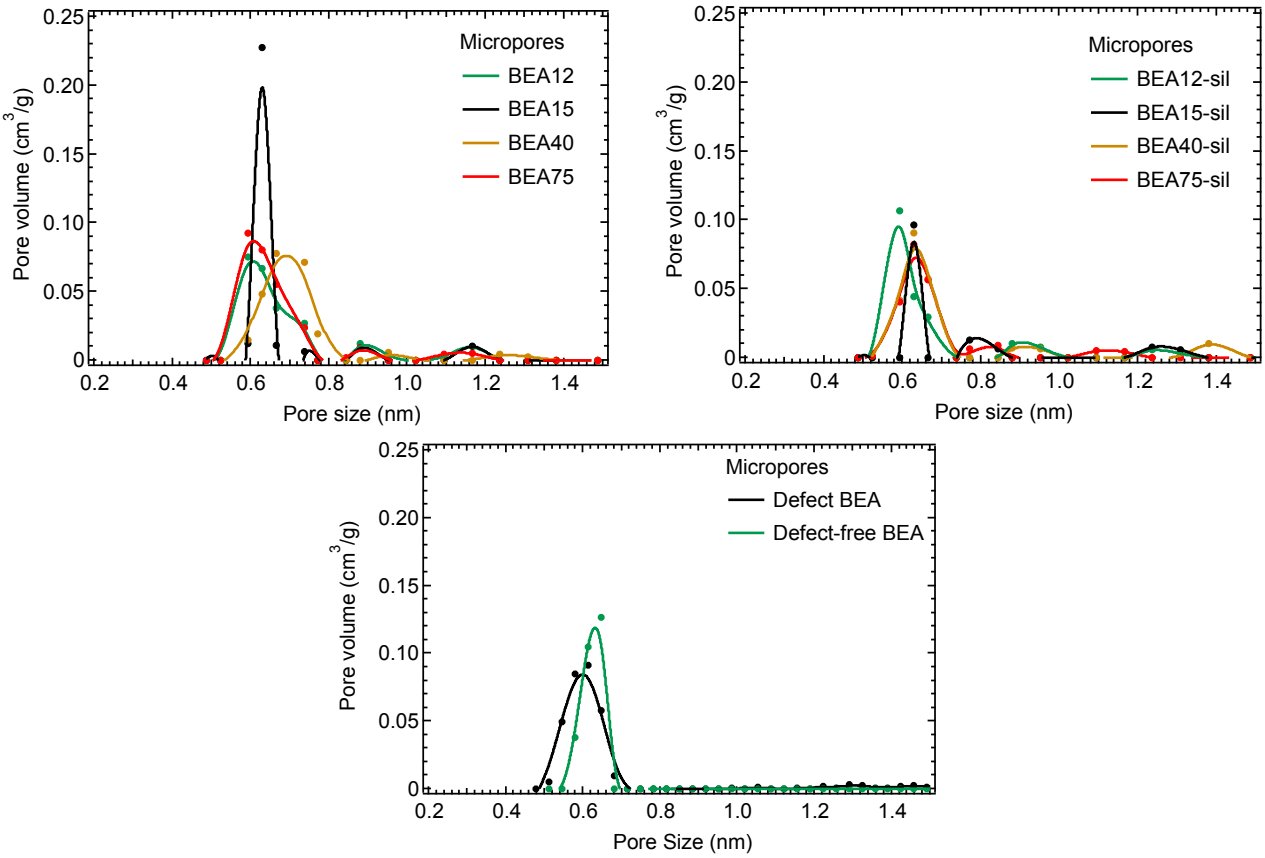

Figure S2. Micropore size distribution for the parent and silylated materials. In the parent materials, there is no clear trend observable. Silylation leads to a reduction of the micropore volume due to the deposition of side products.

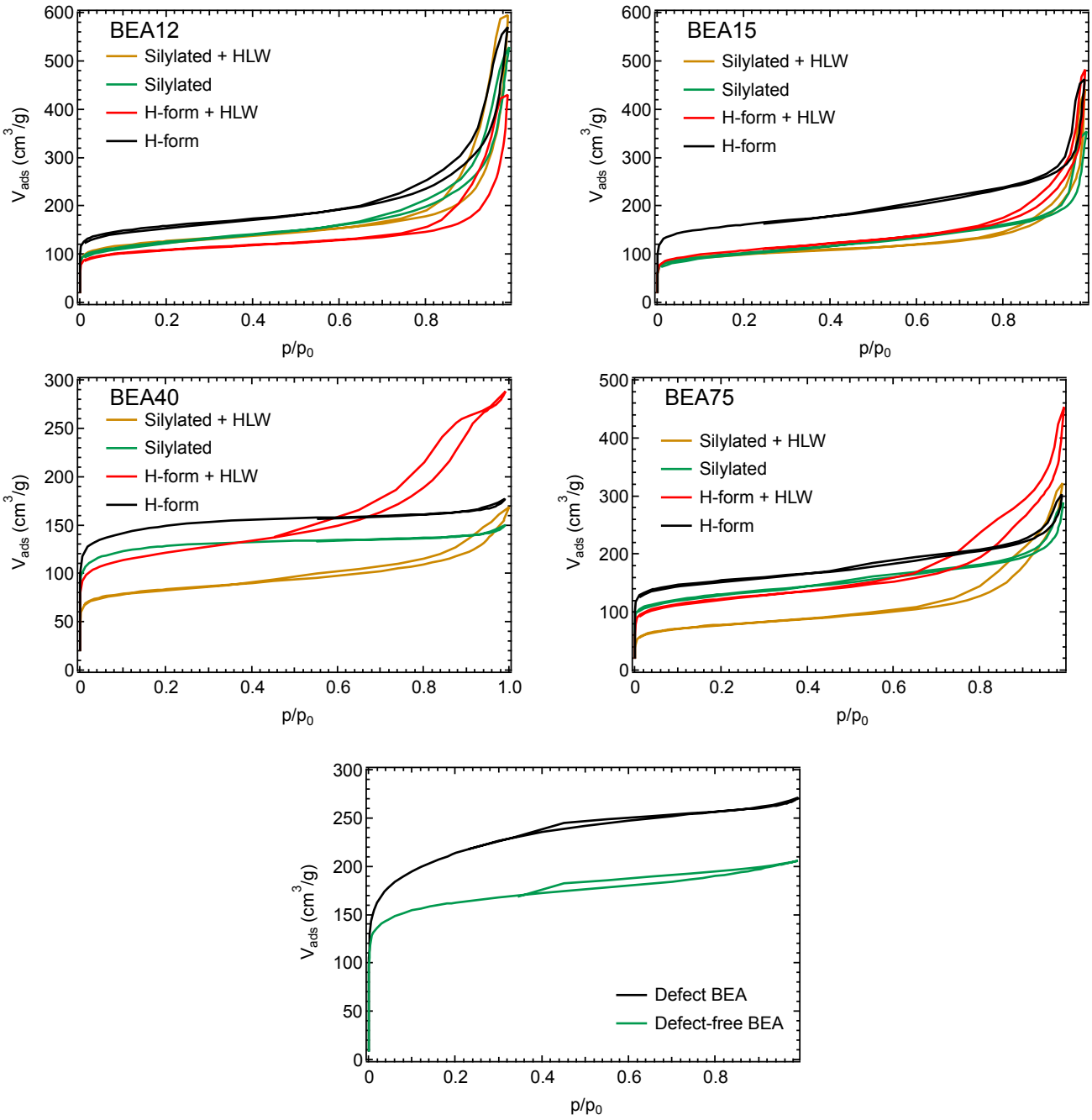

Figure S3. N_2-physisorption isotherms for parent and silylated materials before and after water-treatment. Retention of microporosity upon HLW-treatment is an indicator for stability and can be observed for BEA12 and BEA15 after silylation. BEA40 and BEA75 have an increased mesopore contribution after HLW-treatment due to excessive desilication. At the bottom Ar-physisorption isotherms for defect BEA and defect-free BEA are shown. The corresponding pore volumes are reported in Table S1.

Table S1. BEA samples and their porosities as determined with N_2-physisorption. Total pore volume is determined with single point adsorption close to $p/p_0 = 0.99$. Retention of microporosity after water-treatment is a measure of stability.

Sample	Micropore volume [cm^3/g] DFT	Mesopore volume [cm^3/g]	Total pore volume [cm^3/g]
BEA12	0.23	0.62	0.85
BEA12 + HLW	0.17	0.47	0.64
BEA12-sil	0.18	0.64	0.82
BEA12-sil + HLW	0.18	0.73	0.91
BEA15	0.25	0.48	0.73
BEA15 + HLW	0.13	0.61	0.74
BEA15-sil	0.12	0.42	0.54
BEA15-sil + HLW	0.13	0.53	0.68
BEA40	0.23	0.04	0.27
BEA40 + HLW	0.18	0.30	0.44
BEA40-sil	0.20	0.03	0.23
BEA40-sil + HLW	0.10	0.16	0.26
BEA75	0.25	0.21	0.46
BEA75 + HLW	0.14	0.49	0.64
BEA75-sil	0.15	0.30	0.45
BEA75-sil + HLW	0.09	0.40	0.48
Defect BEA*	0.30	0.05	0.35
Defect-free BEA*	0.28	0.02	0.30

*Samples were measured with Ar-physisorption at 87K.

He ion microscopy

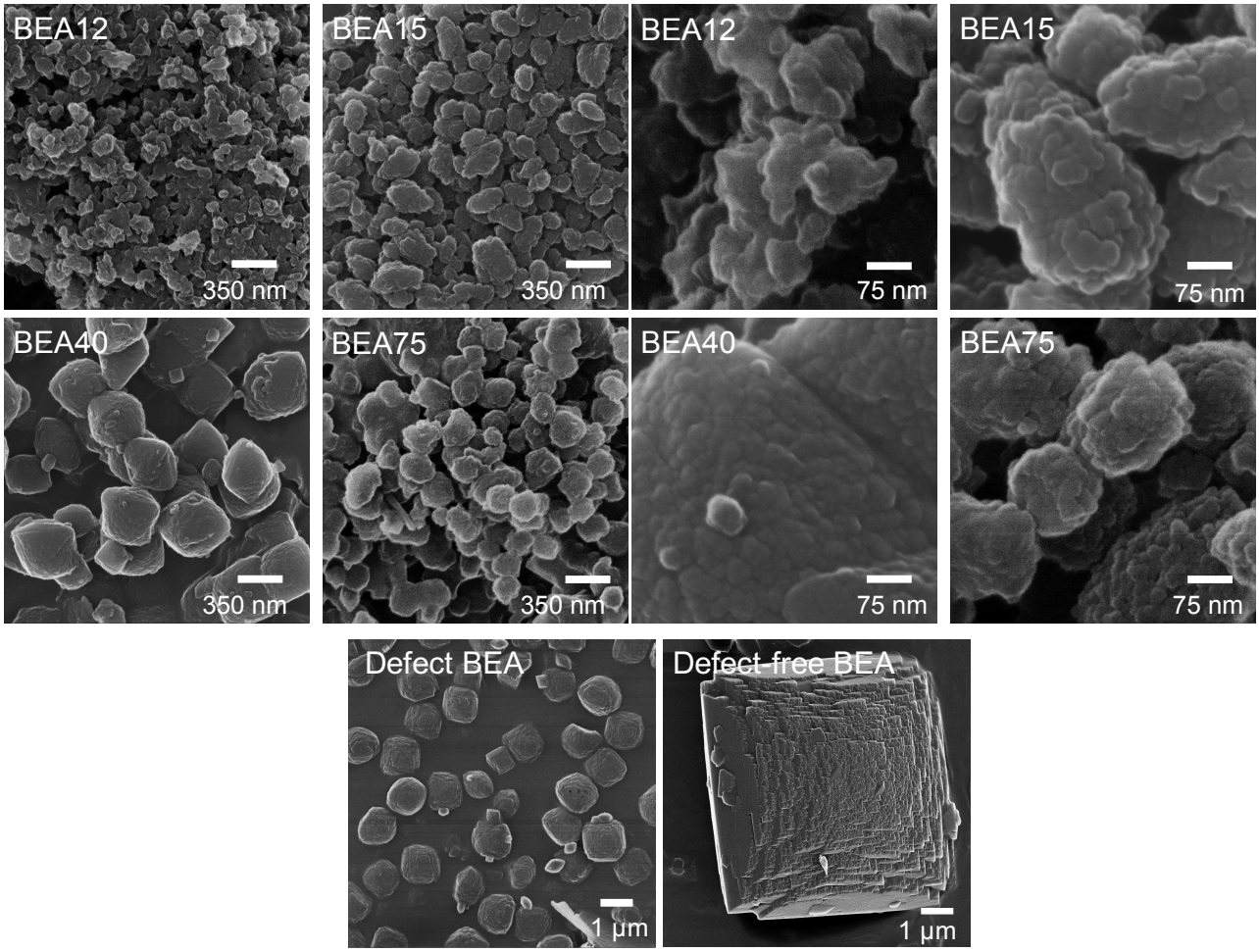

Figure S4. He ion micrographs of BEA samples in their parent form as well as the defect BEA and defect-free BEA. The respective samples are denoted in the legend. Note the much larger particle size of both the defect BEA and defect-free BEA samples.

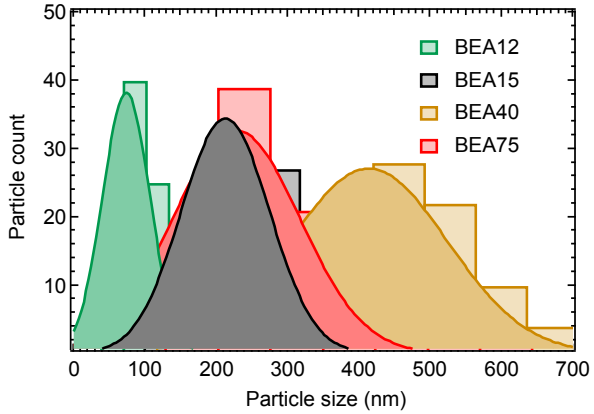

Figure S5. Particle size distribution showing the changes in size as a function of the Si/Al ratio and synthesis method. This is obtained by optically counting and measuring the size of 100 particles. Color-coding is reported in the legend. A Gaussian bell curve is used as a fitting function

^{27}Al MAS NMR and Py-IR quantification

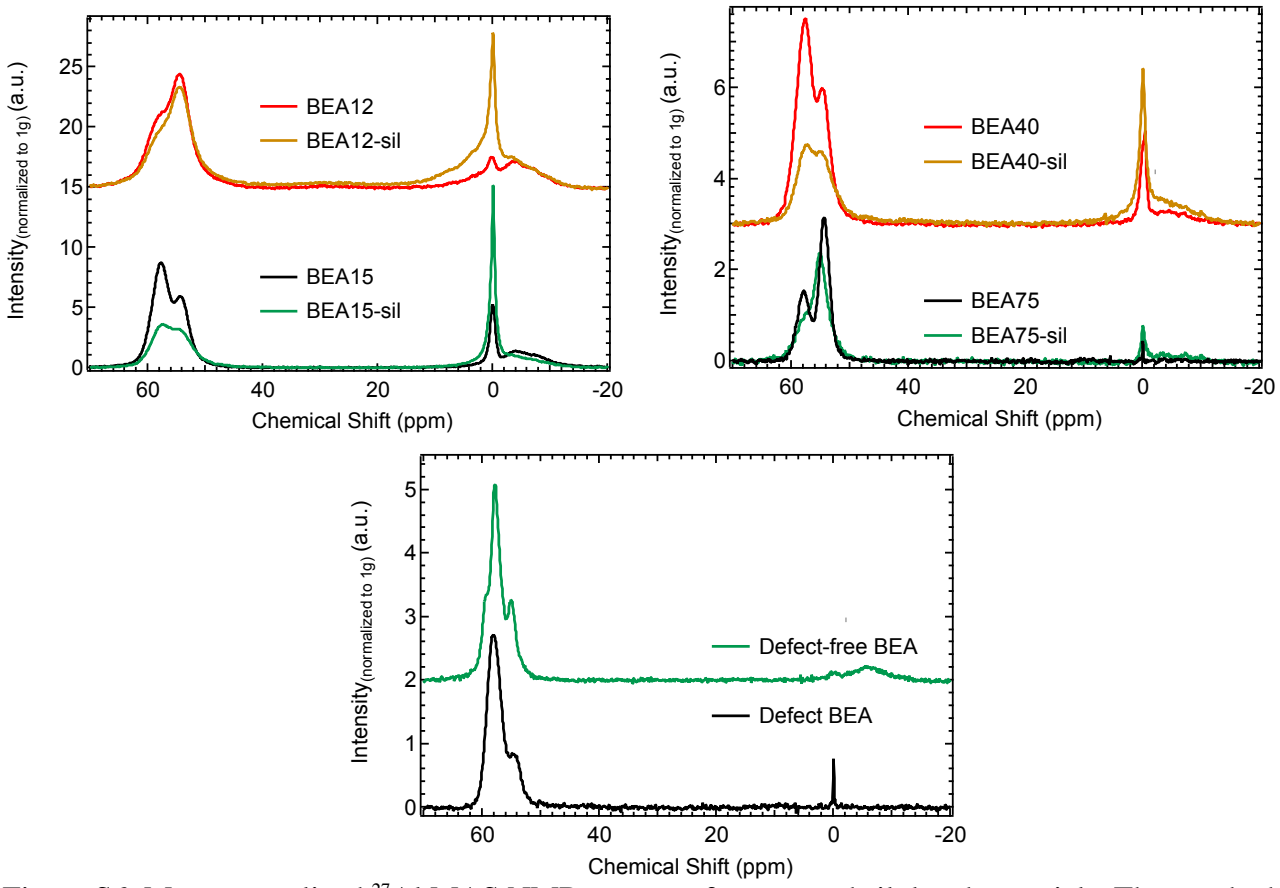

Figure S6. Mass normalized ^{27}Al MAS NMR spectra of parent and silylated materials. The tetrahedral framework Al is represented by the peaks between 54-57 ppm with octahedral species appearing between 0 and -10 ppm. Silylation leads to a selective transformation from tetrahedral Al to octahedral EFAl. At the bottom, defect-free BEA and defect BEA are displayed. Both have only traces of octahedral Al in line with the observations made for the remaining Al-BEA materials. Only the central band is shown.

Table S2. Quantitative analysis of ^{27}Al MAS NMR analyzing the relative distribution of tetrahedral Al^{3+} (IV) and octahedral Al^{3+} (VI) species as well as the total Al concentration (determined by integrating both central and spinning side bands). Additionally, quantitative data of Brønsted and Lewis acidity is also presented. The relative contribution of EFAl and LAS to the total amount of Al/acid sites is reported in the brackets.

Sample	Si/Al_{AAS}	Al_{AAS} [a] (µmol/g)	Al_{NMR} [b] (µmol/g)	Tetrahedral Al^{3+} (µmol/g)	Linewidth IV_A/IV_B [c] (Hz)	Octahedral Al^{3+} (µmol/g)	Brønsted acid sites [d] (µmol/g)	Lewis acid sites[d] (µmol/g)
BEA12	11.9	1340	1190	840	890/1075	310 (26%)	470	475 (50%)
BEA12-sil	12.3	1290	1160	675	1255/1732	475 (41%)	315	250 (44%)
BEA12 + HLW	9.6	1520	1340	1000	1020/930	340 (25%)	505	515 (50%)
BEA15	15.0	1120	910	675	680/750	235 (26%)	540	415 (43%)
BEA15-sil	n/a	n/a	935	485	1045/890	450 (48%)	285	310 (52%)
BEA15 + HLW	n/a	n/a	950	675	985/785	275 (29%)	415	480 (54%)
BEA40	37.8	440	495	400	680/670	95 (19%)	240	120 (33%)
BEA40-sil	40.0	380	460	250	1000/725	210 (46%)	115	100 (46%)
BEA40 + HLW	30.1	505	600	450	490/735	150 (27%)	325	250 (43%)
BEA75	75.0	220	220	215	450/530	5 (2%)	135	32 (19%)
BEA75-sil	n/a	n/a	170	140	640/765	30 (21%)	95	52 (35%)
BEA75 + HLW	n/a	n/a	370	290	735/750	80 (27%)	245	165 (40%)
Defect BEA	150	90	100	97	630/555	3 (3%)	90	20 (18%)
Defect-free BEA	110	165	180	170	490/520	10 (7%)	115	25 (17%)

[a] Determined with AAS [b] Determined using an external standard, BEA75 with known Al concentration from elemental analysis (AAS) [c] Linewidth determined by simple line fitting of Al spectra with mixed Lorentzian-Gaussian (L/G 0.5) function. IV_A and IV_B correspond to the peak at 54 and 57 ppm respectively [d] Quantification using pyridine adsorption.

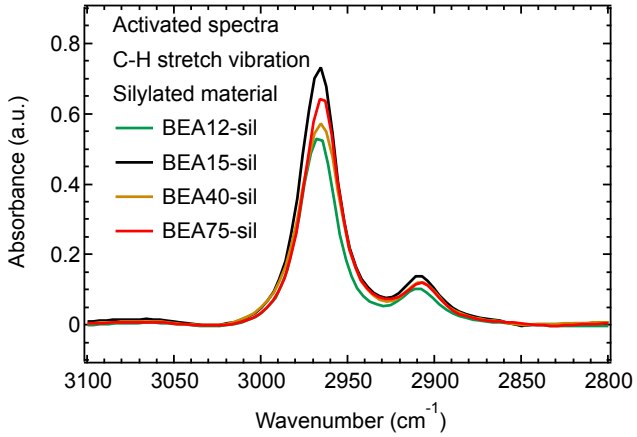

Figure S7. IR spectra of the C-H stretch region for silylated materials. The spectra are normalized to the combination vibrations of the lattice bands between 2090-1740 cm^{-1} (not shown).

Catalysis – conversion plots

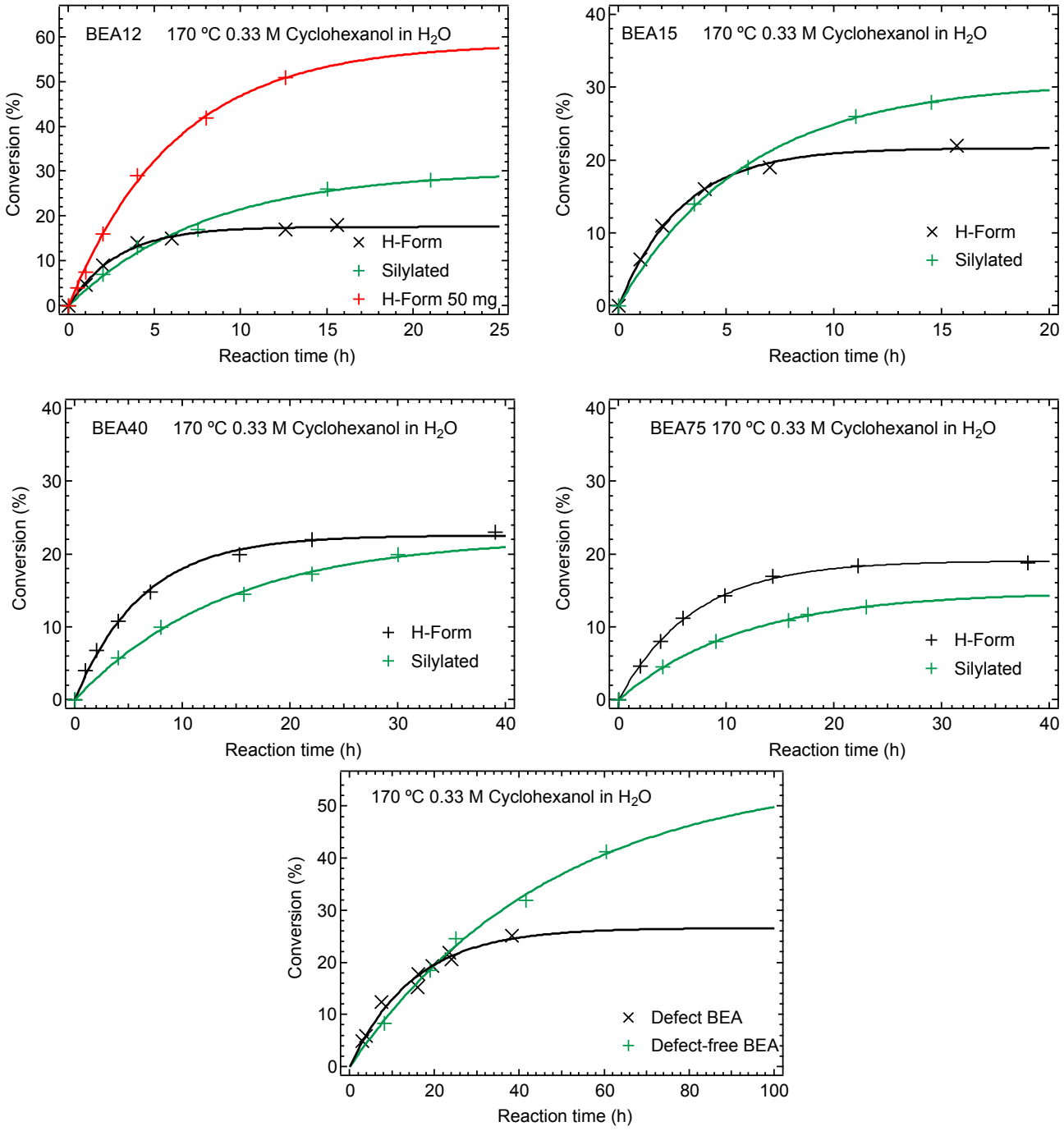

Figure S8. Conversion plots for cyclohexanol dehydration on BEA12, BEA15, BEA40 and BEA75 shown for the parent H-form and silylated materials respectively. Reaction conditions for 30 mg catalyst are reported in the legend. Longer lifetime of silylated materials is evident. Note that using larger amounts of catalyst leads to higher conversion being attained (BEA12 50 mg, red trace, top left). This highlights that the conversion of cyclohexanol in the investigated materials is far from equilibrium. While it is likely to be less than the 87% reported for 200 °C as mentioned in the main text, this experimental evidence proves the equilibrium conversion to still be high. The conversion for the defect-free

BEA and defect BEA are shown at the bottom. Sharing a similar number of active sites, the lifetime and turnover number is determined by the defect concentration, with defect BEA deactivating faster.

Table S3. Derived catalytic properties, i.e. initial rates, turnover frequencies (TOF) and turnover number (TON) for the conversion of cyclohexanol on HBEA zeolite.

Sample	Brønsted acid sites [c] (μmol/g)	Rate [d] ($\mu mol_{Cyclo}/g_{BEA} \cdot s$)	TOF ($mol_{Cyclo}/ mol_{BAS} \cdot s$) $\times 10^{-3}$	Turnover number (TON) (mol_{Cyclo}/ mol_{BAS})	Lifetime (h)
BEA12	470	15.1 ± 1.1	32 ± 4.0	330 ± 34	4.5 ± 0.3
BEA12-sil	315	9.3 ± 1.1	29 ± 4.5	845 ± 92	12.6 ± 1.3
BEA15	540	18.0 ± 1.0	33 ± 3.8	355 ± 36	4.7 ± 0.2
BEA15-sil	285	12.6 ± 0.6	44 ± 5.0	950 ± 96	9.5 ± 0.5
BEA40	240	8.9 ± 0.5	37 ± 4.2	830 ± 84	9.9 ± 0.5
BEA40-sil	115	3.9 ± 0.3	34 ± 4.5	1710 ± 182	22.3 ± 1.8
BEA75	135	6.7 ± 0.2	49 ± 5.1	1250 ± 125	11.0 ± 0.3
BEA75-sil	95	3.2 ± 0.1	33 ± 3.5	1375 ± 138	18.2 ± 0.6
Defect BEA	90	4.4 ± 0.4	49 ± 9.0	2620 ± 330	23.7 ± 3.6
Defect-free BEA	115	2.9 ± 0.3	25 ± 3.0	4365 ± 555	75.0 ± 9.4

[a] Quantification using pyridine adsorption and desorption at 150°C; Accuracy ±10% [b] Initial rate and TOF of cyclohexene formation and catalyst lifetime determined from fitting the conversion-time plots (Fig S8) for 80 mL 0.33 M aqueous cyclohexanol solution at 170 °C, 20 bar H_2 and 30 mg BEA catalyst with an exponential decay function.

All silylated BEA zeolites deactivated more slowly and converted larger amount of cyclohexanol, as seen by an increased TON for all cases. (Table S3). The reduced micropore volume (Table S1 and Figure S3), induced by the silylation, did not prevent access of the reactant molecules to the active hydronium ions; the TOF changed only marginally.

Supporting Note 1 – Zeolite Degradation

Dissolution rate in pure hot liquid water

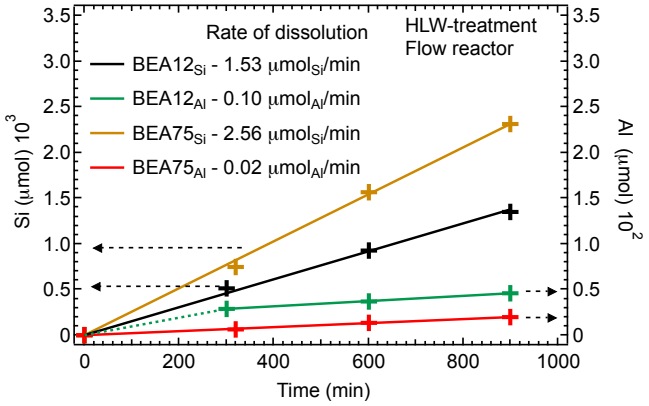

Figure S9. BEA exposed to pure HLW in a trickle bed reactor (200:1, 15h, 10ml/h, 160 °C, 11 bar N_2) elucidated the Si and Al dissolution rates for BEA12 and BEA75. Color-coding and initial rates of Si and Al leaching are reported in the legend.

Deactivation during catalysis

Carbon balance

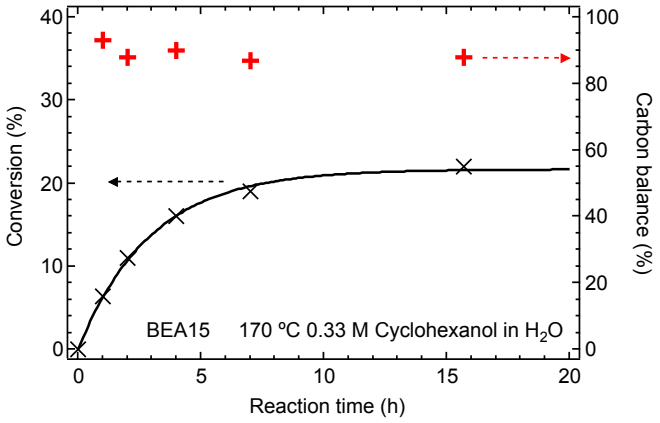

Figure S10. Deactivation of the catalyst during cyclohexanol dehydration and the resultant carbon balance. The carbon balance is less than 100%, due to the formation of volatile cyclohexene as well as uncertainty introducing in the work up procedure. The changes associated with the carbon balance are not significant enough to justify deactivation via coking.

Dissolution of the catalyst

To verify that catalyst deactivation under catalysis conditions occurs via dissolution, a control experiment was conducted with BEA75 using a 0.33 M cyclohexanol solution containing an excessive amount of H_2O compared to the zeolite mass used (2000:1), able to fully dissolve the zeolite, similar to conditions reported for catalytic testing (2600:1). 94% of the zeolite mass was dissolved while the residual amount was analyzed with X-ray diffraction and He ion microscopy, presented below.

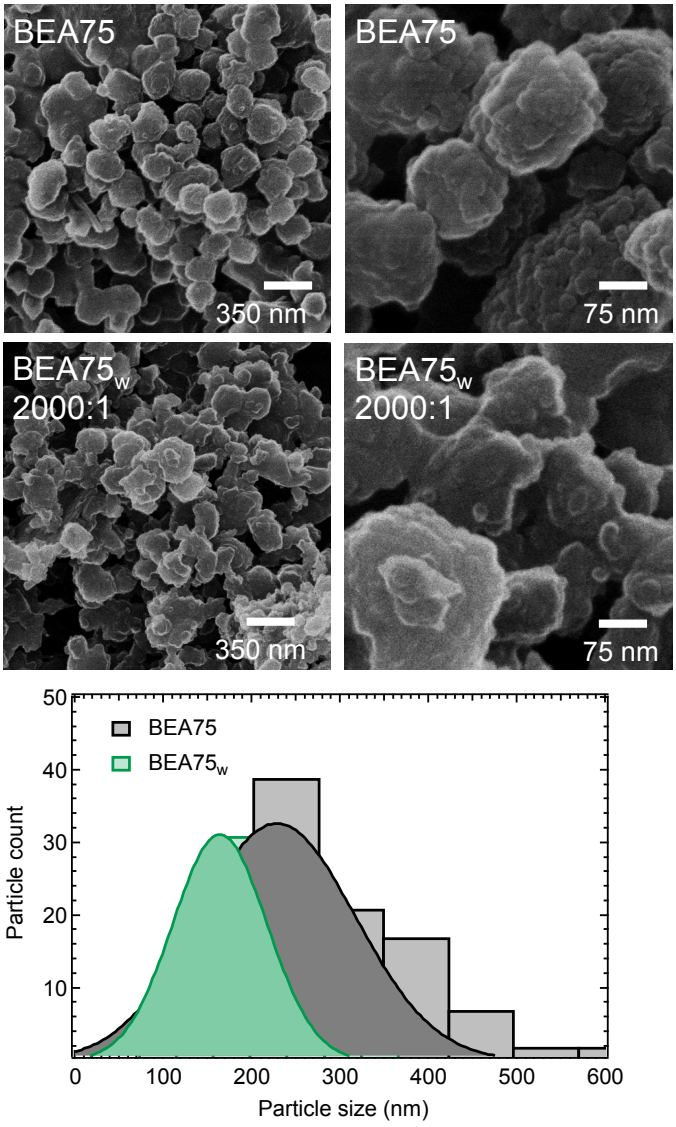

Figure S11. He ion micrographs of BEA75 before and after exposure to excessive amounts of HLW ($BEA75_w$). Residual zeolite presents smoothened surfaces and less round particle morphology. The particle size is also reduced.

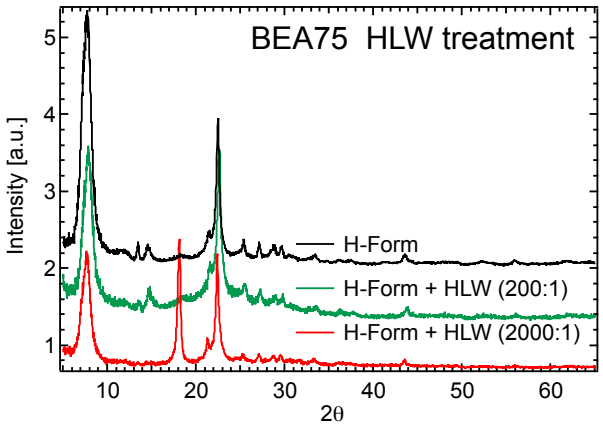

Figure S12. X-ray diffractogram for BEA75 exposed to different amounts of HLW. Conditions typically found for HLW-treatment (200:1) led to partial amorphization due to precipitated SiO_2 (see also Figure S1). Conditions during aqueous phase reactions reported in this publication (2000-2600:1), favor the complete dissolution, with the residual material showing no amorphous component. Instead a reflection at 2θ 18° is observed, tentatively attributed to clay material.

Supporting Note 2 – Liquid phase adsorption

Table S4. Cyclohexanol uptake from a 0.33 M aqueous phase and the corresponding micropore volume occupied by water as measured for room temperature and extrapolated to the reaction temperature of 170 °C. For extrapolation see Figure S13 below. Adsorption of Ar at -186 °C was used to determine the most accurate micropore volume, instead of using the values obtained with N_2 adsorption at -196 °C, shown in Table S1. For BEA15-sil, the accessible micropore volume was determined with gas-phase adsorption of cyclohexanol, which was less than the volume determined with Ar. For all other samples the maximum uptake of cyclohexanol from the gas-phase matched the micropore volume determined with Ar.

Sample	Uptake Cyclohexanol [mmol/g]	Micropore Volume [cm^3/g]	Micropore Concentration Cyclohexanol [$mmol/cm^3$]	Uptake H_2O [mmol/g]	Micropore Concentration H_2O [$mmol/cm^3$]	BAS [mmol/g]
BEA12 - 25 °C	0.77	0.23	3.35	8.32	36.2	0.470
BEA12 - 170 °C	0.49		2.13	9.93	43.2	
BEA75 - 25 °C	1.54	0.27	5.72	6.03	22.4	0.135
BEA75 - 170 °C	1.06		3.94	8.79	32.7	
BEA15 - 25 °C	0.61	0.25	2.44	10.36	41.4	0.540
BEA15 - 170 °C	0.39		1.57	11.61	46.5	
BEA15-sil - 25 °C	0.75	0.15*	5.06	3.88	26.2	0.285
BEA15-sil - 170 °C	0.49		3.29	5.40	36.5	
Defect BEA - 25 °C	1.23	0.30	4.11	9.53	31.8	0.090
Defect-free BEA - 25 °C	2.33	0.28	8.39	1.95	7.0	0.115

* Deduced from the maximum uptake close to p/p_0 for the gas-phase adsorption of cyclohexanol.

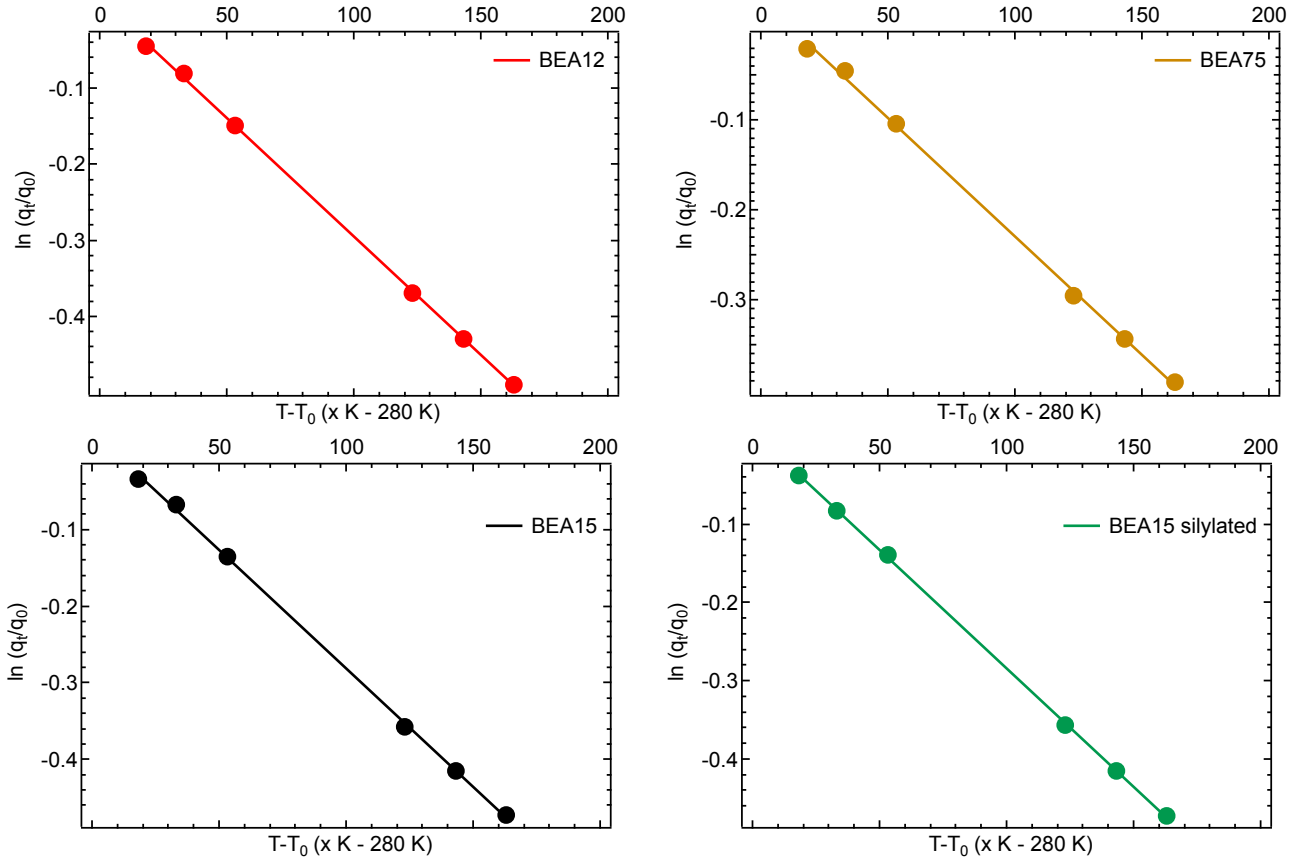

Figure S13. Linearization of the experimentally measured uptakes at low temperatures allows for the extrapolation to reaction temperatures assuming a Langmuir type adsorption process. An explanation for linearization is provided in Liu, Y. *Nat. Commun.* **2017,** 8, 14113.

Supporting Note 3 – Determining the Role of Defects

While it is clearly established that increasing lifetime can be achieved by lowering the Brønsted acid site concentration, the scatter in the low-BAS region suggests that the removal of defects can have a beneficial impact on the lifetime (Figure 5). Therefore, we investigated two additional BEA zeolites. These materials were designed to show the impact of defects, by either having a lot of defects or as little defects as possible. We previously described the generation of a defect-rich model system consisting of the synthesis of a BEA zeolite in hydroxide medium, with boron incorporated. The boron takes the role of the tetrahedral framework unit typically occupied by aluminum. Mild treatment in water resulted in the removal of boron and generation of defect nests. On the other end of the spectrum we synthesized a BEA zeolite in fluoride medium, with a comparable Si/Al and BAS concentration. Fluoride anions have the benefit of compensating the negative framework charge. Therefore the generation of internal defects is avoided. Both materials are pure phase BEA as seen from the X-ray diffractograms in Figure S1. Only a negligible amount of mesopores is observed as the large particles, spanning several micrometers, as seen by He ion micrographs (Figure S4), are isolated without any intracrystalline mesopores. The micropore volume is slightly larger for the defect-BEA owing to the deboronation procedure (Table S1). Only traces of extra-framework octahedral Al are observed (Figure S6). Clearly seen in Figure S8 the defect-free BEA anticipated to have only a negligible concentration of defects shows a superior lifetime, whereas the defect BEA deactivates with time. In respect to the defect concentration, the IR spectra shown below in Figure S14 suggest that defect-free BEA has no isolated or terminal SiOH and a much lower overall intensity in the OH region. Defect-BEA

on the other hand, clearly has signals in the SiOH region attributed to isolated SiOH as well as hydrogen-bonded SiOH at 3500 cm^{-1}.

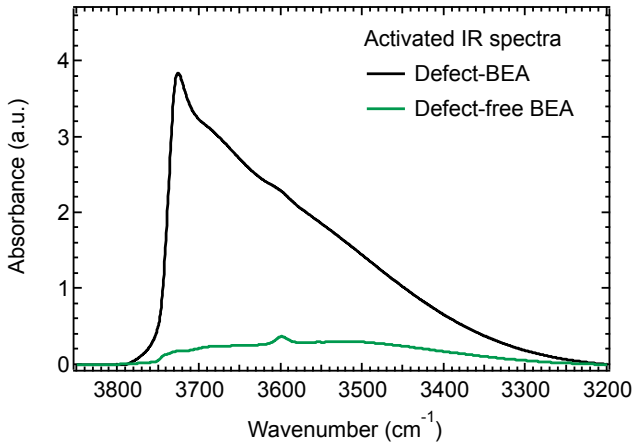

Figure S14. Infrared spectra of both the defect-BEA and defect-free BEA showing the differing degree of hydroxyl groups. The spectra are normalized to the lattice vibrations between 2090-1740 cm^{-1} (not shown).

Furthermore, owing to the small concentration of Al, we could accurately determine the defect concentration for these two materials using ^{29}Si MAS NMR. Rather than the cross-polarization enhanced spectra shown in Figure 2, this quantitative direct pulse measurement allows us to quantify the Q^3 Si. Q^3 Si can either be due to incorporated Al or due to hydroxyl groups connected to the Si, i.e. defect sites. As the particle size is significantly large, the measured SiOH concentration is solely attributed to internal SiOH. Knowing the real concentration of framework Al (e.g. from ^{27}Al MAS NMR) and thus the theoretical amount of Q^3 Si, the difference can be attributed to defects. In principle, this method for determining the defect concentration can be applied to the other investigated materials, however, the increasing concentration of framework Al and the need to deconvolute the spectra leads to a significant degree of inaccuracy. Using this methodology, it is clear that defect-free BEA has no detectable defect concentration as only fully incorporated, Q^4 Si is observed. Defect-BEA on the other hand has a significant Q^3 signal associated with defects. Quantification yielded a concentration of 1100 µmol/g SiOH. The accuracy of this method is ± 10%. Thus it is established that these two compounds are ideal candidates for the deconvolution of the impact of defect concentration on zeolite stability in aqueous phase reactions. They are free of extra-framework Al, have no significant mesopore contribution, a well-defined BAS concentration as well as defect concentrations on two ends of the spectrum.

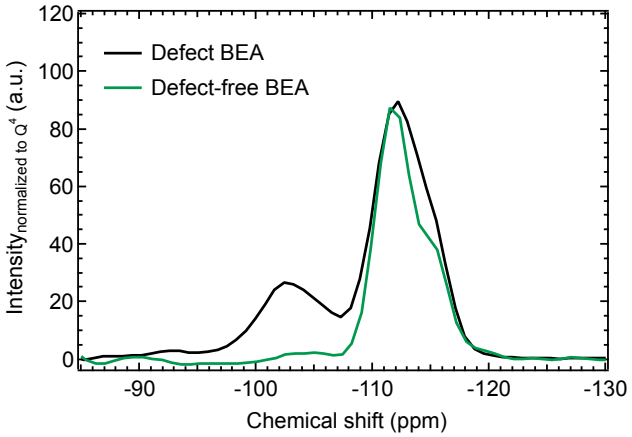

Figure S15. ^{29}Si MAS NMR spectra of the defect and defect-free BEA. The intensity of the Q^3 signal at – 103 ppm is related to the defect concentration of the material. Clearly the defect-free BEA has only a strong signal in the Q^4 region, between -110 and -117 ppm. This way of determining the defect concentration holds for materials with high Si/Al ratios as Q^3 due to Al is negligible.